Tunable Magnonic Chern Bands and Chiral Spin Currents in Magnetic Multilayers

Tunable Magnonic Chern Bands and Chiral Spin Currents in Magnetic Multilayers

Zhongqiang Hu,[1,*] Liang Fu,[2] and Luqiao Liu[1]
[1]Department of Electrical Engineering and Computer Science, Massachusetts Institute of Technology, Cambridge, Massachusetts 02139, USA
[2]Department of Physics, Massachusetts Institute of Technology, Cambridge, Massachusetts 02139, USA

(Received 3 January 2022; revised 21 March 2022; accepted 28 April 2022; published 23 May 2022)

Realization of novel topological phases in magnonic band structures represents a new opportunity for the development of spintronics and magnonics with low power consumption. In this work, we show that in antiparallelly aligned magnetic multilayers, the long-range, chiral dipolar interaction between propagating magnons generates bulk bands with nonzero Chern integers and magnonic surface states carrying chiral spin currents. The surface states are highly localized and can be easily toggled between nontrivial and trivial phases through an external magnetic field. The realization of chiral surface spin currents in this dipolarly coupled heterostructure represents a magnonic implementation of the coupled wire model that has been extensively explored in electronic systems. Our work presents an easy-to-implement system for realizing topological magnonic surface states and low-dissipation spin current transport in a tunable manner.

DOI: 10.1103/PhysRevLett.128.217201

Exploration of novel topological phases in quantum matter has become one of the central topics in current condensed matter research, opening up avenues towards electronics with high speed and low power consumption [1–5]. Beyond electronic systems, recently topological phases have also been generalized to various bosonic systems, including phononic [6,7] and photonic [8,9] crystals. Magnon, the quantized collective excitation of localized spins, represents a promising candidate for efficient spin transport [10–12]. However, the inevitable scattering from phonons, impurities as well as among magnons themselves, deflects magnons into different directions, greatly limiting the coherence length of spin waves and preventing long-range spin signal transfer [13–16]. The formation of topological magnonic surface states with suppressed scattering is therefore of great importance for realizing low-dissipation magnonic devices, which has been proposed in several works [17–25]. Nevertheless, these proposals require materials with either special crystal symmetries [17–22] or artificially modulated structures that demand advanced nanofabrication techniques [23–25], both of which bring in difficulties for experimental realization.

In this Letter, we theoretically study the magnonic band structure and corresponding topological properties of antiparallelly aligned magnetic multilayers. We find that the long-range dipolar interaction between propagating magnons is chiral in nature, whose strength depends on the wave vector direction and therefore breaks time-reversal symmetry (TRS). Previously, the dipolar interaction has been utilized to modulate the magnon transport properties and induce the magnon spin or thermal Hall effect in both ferromagnets [26] and antiferromagnets [27], as well as been discovered to account for the topological origin of magnetostatic surface spin waves [28,29]. Here we show that, by correlating the sublattice and momentum degrees of freedom, the dipolar interaction generates bulk bands with nonzero Chern integers and ultralocalized magnonic surface states that carry chiral spin currents. Through an external magnetic field, the topological phase of the magnonic band can be switched, which therefore provides a tunable and efficient way for transferring spin angular momenta in this synthetic antiparallelly aligned heterostructure.

The magnetic multilayers we study are shown in Fig. 1(a), where the neighboring layers possess antiparallel equilibrium magnetic moments due to antiferromagnetic interfacial exchange, as demonstrated in several recent experiments [30–32]. An external magnetic field applied along the y axis always aligns the higher- (lower-) moment layers parallel (antiparallel) to it. The external field strength is below the critical value for any spin-flop transition, ensuring the stability of antiparallel configuration throughout the Letter. The layers with the same equilibrium moment orientations have entirely identical properties including their material composition and thickness, providing the system with periodicity along the z direction, and allowing us to define unit cells with thickness of $d = d_1 + d_2$, as shown in red frames in Fig. 1(a).

We start by considering the simplified case, where the magnetic moment distribution along the y and z axes within the same layer is uniform, i.e., the lowest-order standing wave mode. Consequently, magnons are confined to transport along the x axis in each individual layer. Meanwhile, it is assumed that each layer is infinitely long along the x axis, which is applicable to the regions far away from film edges

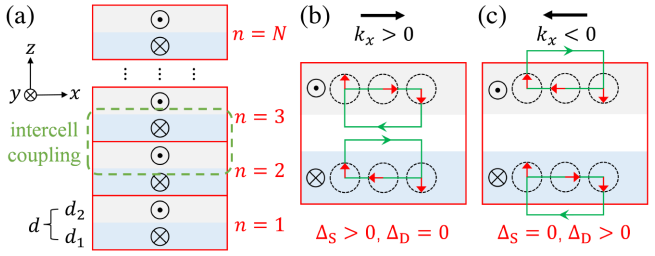

FIG. 1. (a) Scheme of antiparallelly aligned magnetic multilayers. The blue (gray) blocks with thickness of $d_{1(2)}$ form the 1st (2nd) sublattice. The equilibrium moments in the 1st (2nd) sublattice are parallel to the $+y$ ($-y$) direction, represented by $\otimes$ ($\odot$) symbols. The red, solid frames correspond to unit cells (indexed by $n = 1, 2, \ldots, N$) with thickness of $d = d_1 + d_2$. The green, dotted frames select two layers belonging to neighboring cells with intercell dipolar coupling. (b) Scheme of dipolar fields (green lines and arrows) generated by propagating magnons with $k_x > 0$ in two layers within a cell. The red arrows represent the deviations of magnetic moments from their equilibrium orientations, which propagates from left to right as a function of time (the traces are represented by black, dotted circles). Here, the two layers experience finite dipolar fields from each other, corresponding to $\Delta_S > 0$. Meanwhile, they experience zero dipolar fields from magnons in the layers of neighboring cells, corresponding to $\Delta_D = 0$. (c) Scheme of dipolar fields generated by propagating magnons with $k_x < 0$ for two layers within a cell, corresponding to $\Delta_S = 0$ and $\Delta_D > 0$.

in the real world. Considering intrinsic exchange modes in the absence of interlayer interactions, we can write the magnonic Hamiltonian for the multilayers as $\hat{\mathcal{H}}_0 = \sum_{k_x,j,n} \omega_j b^\dagger_{jn,k_x} b_{jn,k_x}$, where $b^\dagger_{jn,k_x}$ is the creation operator for a circularly polarized magnon with wave vector k_x in the jth layer ($j = 1, 2$ for sublattice indices) of the nth cell ($n = 1, 2, \ldots, N$ for cell indices), and $\omega_j = A_j k_x^2 + \Omega_j$ stems from the intralayer exchange interaction and the effective static field experienced by each sublattice [33]. Here, the coefficient A_j is defined as $A_j = 2A_j^{\mathrm{ex}}\gamma/M_{sj}$, with the exchange stiffness constant A_j^{ex}, electron's gyromagnetic ratio γ, and the saturated magnetization M_{sj}, while $\Omega_j = \gamma\mu_0 H_j$ is the Larmor precession frequency, with vacuum permeability μ_0, and the effective static field H_j. Because of the dipolar interaction, magnons in neighboring layers will get coupled. As previous studies reveal [37–40], one important feature associated with the dipolar field from propagating magnons is the chirality—whether it emerges on the top or bottom side of the thin film depends on the sign of k_x and the equilibrium moment orientation, as illustrated in Figs. 1(b) and 1(c). With the nearest neighboring approximation [33], the dipolar interaction Hamiltonian for the multilayers can be written as $\hat{\mathcal{H}}_{\mathrm{int}} = \sum_{k_x,n}(\Delta_S b^\dagger_{1n,k_x} b_{2n,k_x} + \Delta_D b^\dagger_{1n,k_x} b_{2,n-1,k_x} + \mathrm{H.c.})$, with the intracell (intercell) coupling strength $\Delta_{S(D)}$. When $|k_x|$ is not large compared with the Brillouin zone (BZ) boundary, $\Delta_{S(D)} = B \cdot (|k_x| \pm k_x)$, with $B = \gamma\mu_0 N_1 N_2 \sqrt{M_{s1} d_1 M_{s2} d_2}/2$ and $N_j = (1 - e^{-|k_x| d_j})/(|k_x| d_j)$ [33]. In sharp contrast to the standard analytic expressions that describe local interactions in electronic systems, $\Delta_{S(D)}$ here contains a nonanalytic function of $|k_x| \pm k_x$, which is originated from the long-range nature of dipolar fields.

Combining $\hat{\mathcal{H}}_0$ and $\hat{\mathcal{H}}_{\mathrm{int}}$, adopting periodic boundary condition (PBC) along the z axis, and implementing Fourier transformation, i.e., $b_{jn,k_x} = (1/\sqrt{N})\sum_{k_z} \beta_{j,\boldsymbol{k}} e^{ik_z nd}$ with $\boldsymbol{k} = k_x\hat{x} + k_z\hat{z}$, we get the bulk magnonic Hamiltonian for the multilayers on the basis of $\boldsymbol{\beta}_{\boldsymbol{k}} = [\beta_{1,\boldsymbol{k}}, \beta_{2,\boldsymbol{k}}]^T$:

$$\hat{\mathcal{H}}_{\mathrm{bulk}} = \sum_{\boldsymbol{k}} \boldsymbol{\beta}^\dagger_{\boldsymbol{k}} \boldsymbol{H}_{\mathrm{bulk}}(\boldsymbol{k}) \boldsymbol{\beta}_{\boldsymbol{k}},$$
$$\boldsymbol{H}_{\mathrm{bulk}}(\boldsymbol{k}) = \begin{bmatrix} \omega_1 & \Delta_S + \Delta_D e^{-ik_z d} \\ \Delta_S + \Delta_D e^{ik_z d} & \omega_2 \end{bmatrix}. \quad (1)$$

Equation (1) coincides with the expression of the celebrated one-dimensional Su-Schrieffer-Heeger (1D SSH) model [41], except that our model applies to a two-dimensional (2D) case with both ω_j and $\Delta_{S(D)}$ being functions of k_x. In the SSH model, the existence of surface or edge states is determined by the relative magnitude of Δ_S and Δ_D. In our case, this is further controlled by the sign of k_x, as one can easily verify $\Delta_S > \Delta_D$ for $k_x > 0$, and $\Delta_S < \Delta_D$ for $k_x < 0$. Solving the eigenvalue equation $\boldsymbol{H}_{\mathrm{bulk}}|\chi\rangle = \omega|\chi\rangle$, we can get the higher (lower) eigenfrequency $\omega_\pm = (\omega_1 + \omega_2)/2 \pm \sqrt{(\omega_1 - \omega_2)^2/4 + 4B^2 k_x^2}$, either of which has no dispersions along the k_z direction, suggesting a flat band when k_x is fixed. Since our model is 2D in the xz plane with broken TRS, we can calculate the Chern integer as the topological invariant. Denoting $|\chi_-\rangle$ as the eigenstate corresponding to ω_-, we can calculate the Chern integer $\mathrm{Ch}_- = (2\pi)^{-1} \iint_{\mathrm{BZ}} \Omega_-(\boldsymbol{k}) dk_x dk_z$ for the lower band, where $\Omega_-(\boldsymbol{k}) = i\partial_{k_x}\langle\chi_-|\partial_{k_z}|\chi_-\rangle - i\partial_{k_z}\langle\chi_-|\partial_{k_x}|\chi_-\rangle$ is the Berry curvature. The Chern integer is evaluated to be

$$\mathrm{Ch}_- = \begin{cases} 1 & (A_1 > A_2, H_1 < H_2) \\ -1 & (A_1 < A_2, H_1 > H_2) \\ 0 & (\text{otherwise}) \end{cases}, \quad (2)$$

suggesting that the bulk bands possess nonzero Chern integers when $(A_1 - A_2)(H_1 - H_2) < 0$.

The surface states can be explicitly obtained by considering multilayers with open boundary condition (OBC) along the z direction. The magnonic Hamiltonian for the N-cell multilayers is $\hat{\mathcal{H}} = \hat{\mathcal{H}}_0 + \hat{\mathcal{H}}_{\mathrm{int}} = \sum_{k_x} \boldsymbol{b}^\dagger_{k_x} \boldsymbol{H}(k_x) \boldsymbol{b}_{k_x}$, where $\boldsymbol{b}_{k_x} = [b_{11,k_x}, b_{21,k_x}, \ldots, b_{1N,k_x}, b_{2N,k_x}]^T$ and $\boldsymbol{H}(k_x)$ is a $2N \times 2N$ matrix. Solving the eigenvalue equation $\boldsymbol{H}|\chi\rangle = \omega|\chi\rangle$, we can get $2N$ eigenfrequencies and corresponding eigenstates. When $k_x < 0$, corresponding to $\Delta_S = 0$ and $\Delta_D > 0$, two surface states emerge, which

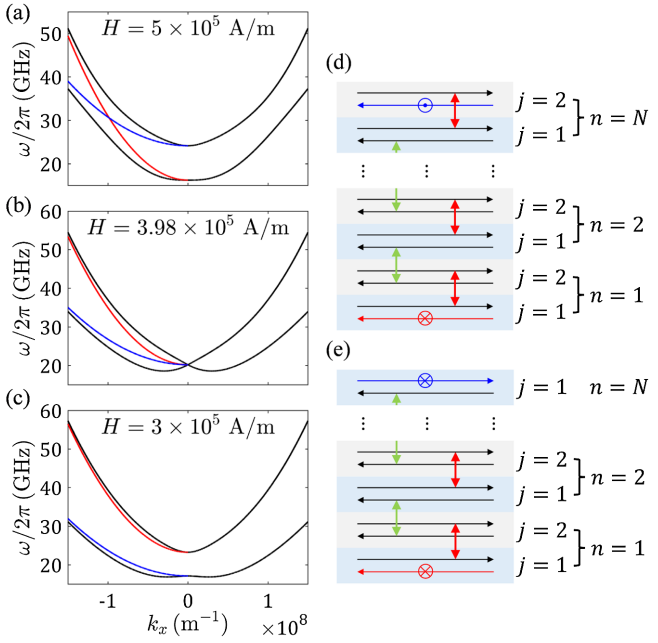

FIG. 2. (a)–(c) Evolution of the magnonic band structure with a varying external field H. The black lines correspond to bulk states, and the red (blue) line corresponds to the surface state localized in the bottom (top) layer. (a) and (c) The topologically nontrivial and trivial phases, respectively. (b) The topological transition. (d) Coupled wire construction with $2N$ total layers. Because of the chirality of the interlayer dipolar interaction, right-moving magnons get coupled (red arrows) within the same cell, while left-moving magnons get coupled (green arrows) between neighboring cells. Two surface states are therefore left uncoupled, on which the symbols of $\otimes$ and $\odot$ show the orientations of carried spins. (e) Coupled wire construction with $2N-1$ total layers.

are separately localized in the 1st layer of the 1st cell (bottom layer) with $\omega^{1e} = \omega_1$, $|\chi^{1e}\rangle = [1, 0, 0, \ldots, 0]^T$, and in the 2nd layer of the Nth cell (top layer) with $\omega^{2e} = \omega_2$, $|\chi^{2e}\rangle = [0, 0, \ldots, 0, 1]^T$. We note that both of them are localized on the surfaces with little decay into the bulk. Figures 2(a)–2(c) show the evolution of the magnonic band structure, with a varying external field H. In this calculation, we consider an example consisting of alternating 10 nm yttrium iron garnet (YIG, 1st sublattice) and 10 nm permalloy (Py, 2nd sublattice) thin films, with reported material parameters of $A_1^{ex} = 3.7 \times 10^{-12}$ J/m, $A_2^{ex} = 8.7 \times 10^{-12}$ J/m, $M_{s1} = 1.4 \times 10^5$ A/m, and $M_{s2} = 7.4 \times 10^5$ A/m [42,43]. An external magnetic field is assumed along the -y direction. The antiferromagnetic exchange coupling constant at the YIG/Py interface is taken to be $J = -8.6 \times 10^4$ J/m^2 [32], which gives rise to the static interfacial exchange field $H_j^{ex} = 2|J|/(\mu_0 M_{sj} d_j)$ experienced by each sublattice, further leading to the total effective static field $H_j = H_j^{ex} \mp H$. As the Chern integer calculation shows, the topology of the magnonic band depends on the sign of $(A_1 - A_2)(H_1 - H_2)$, which can be further controlled by tuning the relative magnitude of H_1 and H_2 through H, given that $A_1 - A_2 > 0$ is fixed. In Fig. 2(a), under $H = 5 \times 10^5$ A/m, corresponding to $H_1 < H_2$, the bulk bands (black lines) are inverted around $k_x = 0$ and two surface bands (red and blue lines) emerge in the $k_x < 0$ half-space, which cross each other and form a degenerate point, i.e., a tilted Dirac cone, without pairing at its time-reversal point due to broken TRS. When H is reduced such that $H_1 = H_2$, a topological transition happens [Fig. 2(b)], where the bulk bands become degenerate at $k_x = 0$, corresponding to a gap closing. With further decreasing H such that $H_1 > H_2$ [Fig. 2(c)], there is no bulk band inversion and the surface bands do not cross each other in the $k_x < 0$ half-space, representing a topologically trivial system.

The formation of ultralocalized surface states in the magnetic multilayers can be further understood as a magnonic implementation of the coupled wire model that has been widely investigated in the circumstance of quantum Hall effect (QHE) in electronic systems [44–47]. We begin by regarding the multilayers as an array of $2N$ noninteracting one-dimensional wires, with single-particle magnonic dispersion relations $\omega_{1(2)}(k_x)$, which cross each other in the condition of $(A_1 - A_2)(H_1 - H_2) < 0$. Because of the interlayer dipolar interaction, magnons around the band-crossing points in neighboring layers get coupled, as shown in Fig. 2(d). As discussed earlier, depending on the sign of k_x, either Δ_S or Δ_D reduces to zero. For right-moving magnons ($k_x > 0$), $\Delta_D = 0$ and $\Delta_S > 0$, the coupling only happens within the same cell [red arrows in Fig. 2(d)], while for left-moving magnons ($k_x < 0$), $\Delta_S = 0$ and $\Delta_D > 0$, the coupling only happens between neighboring cells (green arrows). Consequently, the left-moving magnons in the bottom and top layers are left uncoupled and form a pair of surface states. Considering that two surface layers possess opposite equilibrium moments, the surface magnonic states would carry spin currents with opposite directions. This kind of chiral surface spin currents still exist even if the number of layers is odd, as shown in Fig. 2(e). In this case, the surface states have opposite velocities but the same equilibrium moment orientations, hence still carrying opposite spin currents. The formation of surface magnonic states and chiral spin currents here is similar to the realization of QHE in electronic systems, where the left- and right-moving electrons in neighboring wires are coupled together due to interchannel scattering.

Until now, we have demonstrated tunable magnonic Chern bands and ultralocalized surface states carrying chiral spin currents in the 2D simplified case. In the following, we extend our discussion to a generic case where magnons can propagate within the whole xy plane in each individual layer, i.e., with in-plane momenta $\boldsymbol{k}_\parallel = k_x\hat{x} + k_y\hat{y}$, and both the intralayer dipolar interaction and dynamic interfacial exchange interaction are included. With PBC along the z axis, the bulk magnonic Hamiltonian

for the three-dimensional (3D) multilayers can be expressed in the Bogoliubov–de Gennes formalism:

$$\hat{\mathcal{H}}'_{\rm bulk} = \frac{1}{2}\sum_{\boldsymbol{k}} [\boldsymbol{\beta}^\dagger_{\boldsymbol{k}} \quad \boldsymbol{\beta}_{-\boldsymbol{k}}]\, \boldsymbol{H}'_{\rm bulk}(\boldsymbol{k}) \begin{bmatrix} \boldsymbol{\beta}_{\boldsymbol{k}} \\ \boldsymbol{\beta}^\dagger_{-\boldsymbol{k}} \end{bmatrix},$$
$$\boldsymbol{H}'_{\rm bulk}(\boldsymbol{k}) = \begin{bmatrix} \boldsymbol{h}(\boldsymbol{k}) & \boldsymbol{b}(\boldsymbol{k}) \\ \boldsymbol{b}^*(-\boldsymbol{k}) & \boldsymbol{h}^*(-\boldsymbol{k}) \end{bmatrix}, \tag{3}$$

with $\boldsymbol{k} = \boldsymbol{k}_\parallel + k_z\hat{z}$. The diagonal block $\boldsymbol{h}(\boldsymbol{k})$ in Eq. (3) has the form of

$$\boldsymbol{h}(\boldsymbol{k}) = \begin{bmatrix} \omega'_1 & \Delta'_S + \Delta'_D e^{-ik_z d} \\ \Delta'_S + \Delta'_D e^{ik_z d} & \omega'_2 \end{bmatrix}, \tag{4}$$

with

$$\omega'_j = A_j \boldsymbol{k}^2_\parallel + \Omega_j + \frac{\gamma\mu_0 M_{sj}}{2}\left[(1-N'_j)\frac{k_x^2}{k^2_\parallel} + N'_j\right],$$
$$\Delta'_{S(D)} = \frac{B'}{2}\cdot\left(k_\parallel + \frac{k_x^2}{k_\parallel} \pm 2k_x\right), \tag{5}$$

where N'_j and B' are obtained by replacing $|k_x|$ with $|\boldsymbol{k}_\parallel|$ in N_j and B. The off-diagonal block $\boldsymbol{b}(\boldsymbol{k})$ in Eq. (3) has the form of

$$\boldsymbol{b}(\boldsymbol{k}) = \begin{bmatrix} \delta_1 & \delta'\cdot(1+e^{-ik_z d}) \\ \delta'\cdot(1+e^{ik_z d}) & \delta_2 \end{bmatrix}, \tag{6}$$

with

$$\delta_j = \frac{\gamma\mu_0 M_{sj}}{2}\left[(1-N'_j)\frac{k_x^2}{k^2_\parallel} - N'_j\right],$$
$$\delta' = \frac{\gamma\mu_0}{2}\prod_{j=1,2}\left[f'_j\cdot(k_\parallel - \frac{k_x^2}{k_\parallel}) + H_j^{\rm ex}\right]^{1/2}, \tag{7}$$

where $f'_{1(2)} = M_{s2(1)}d_{2(1)}N'_1N'_2/2$. The derivation for Eqs. (3)–(7) is presented in Ref. [33]. Here, we note that the intralayer dipolar interaction not only modifies ω'_j by adding a term proportional to M_{sj}, but also mixes magnon modes with opposite handedness, i.e., particles and holes, within the same layer, leading to nonzero δ_j in $\boldsymbol{b}(\boldsymbol{k})$. One can also verify that the contribution of the static intralayer dipolar field (also known as demagnetization field) changes the total effective field from H_j to $\sqrt{H_j(H_j+M_{sj})}$. On the other hand, the dynamic interfacial exchange interaction and the interlayer dipolar interaction under finite k_y give rise to the terms proportional to δ' in $\boldsymbol{b}(\boldsymbol{k})$, coupling magnon modes with opposite handedness in neighboring layers. For the usual cases with large enough effective static field that we are interested in, the difference between frequencies of right- and left-handed magnon modes is large, so $\boldsymbol{b}(\boldsymbol{k})$ in Eq. (3) plays a role as a weak perturbation, which does not lead to extra band inversions. Therefore approximately, the existence of surface states is still governed by the relative magnitude of Δ'_S and Δ'_D in $\boldsymbol{h}(\boldsymbol{k})$, which is further controlled by the sign of k_x according to Eq. (5).

With OBC along the z direction, the magnonic band structure can be solved through numerical methods based on the Cholesky decomposition [48]. Using the same parameters as in Figs. 2(a)–2(c), we plot the magnonic band structure in Figs. 3(a)–3(d) with fixed k_y for two different H, when all the interactions are included. We see that after extending to a generic 3D case, the surface states still exist in the $k_x < 0$ half-space. When H remains the same and k_y varies, the magnonic band keeps its topological properties, either with nontrivial [Figs. 3(a) and 3(b)] or trivial [Figs. 3(c) and 3(d)] surface states, suggesting that the 3D multilayers can be regarded as the magnonic analog of stacked 2D Chern "insulators" along the y direction [49]. Similar to the 2D case discussed earlier, the topological phases are still tunable through H, as illustrated by the comparison of Figs. 3(a) and 3(c). The subtle difference for the 3D case is that with finite k_y, Δ'_S no longer vanishes for $k_x < 0$, and the surface states therefore extend into the bulk with an exponential decay in magnitude, $|\chi^{1e}\rangle(z) \sim e^{-z/\xi}$

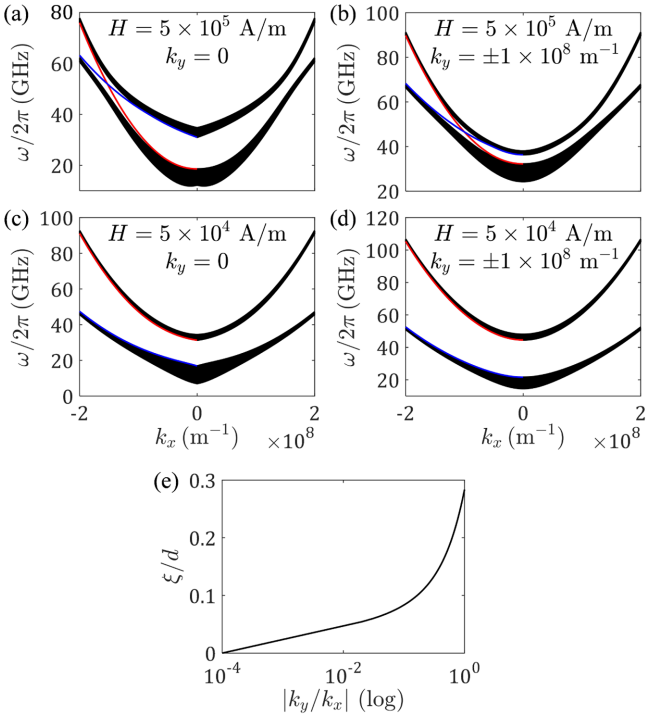

FIG. 3. (a)–(d) Magnonic band structure for 3D multilayers with $N = 20$ cells when all the interactions are included. Panels (a) and (b) correspond to the topologically nontrivial phase with $H = 5\times10^5$ A/m, while (c) and (d) correspond to the trivial phase with $H = 5\times10^4$ A/m. k_y is fixed at 0 for (a) and (c), and is fixed at $\pm1.0\times10^8$ m^{-1} for (b) and (d). (e) Decay length ξ of surface states as a function of $|k_y/k_x|$.

and $|\chi^{2e}\rangle(z) \sim e^{-(z-Nd)/\xi}$, where $\xi = d/\log(\Delta'_D/\Delta'_S)$ is the decay length plotted in Fig. 3(e). $\xi \ll d$ for $k_y < k_x$ indicates the surfaces states are still highly localized.

In order to experimentally identify the topological phases, one can characterize the magnonic band structure using Brillouin-light-scattering spectroscopy [50], to pinpoint the surface states in the gap of bulk states, as predicted in Figs. 2 and 3. Meanwhile, when the system is in the nontrivial phase, one can observe the perfect nonreciprocity and enhanced coherence length of topological surface magnons by measuring magnon transmission with propagating spin wave spectroscopy [12,51]. To further show the viability of these proposed experimental approaches, we carry out micromagnetic simulations using the standard micromagnetic package MuMax3 [33,52], which shows magnonic bands and surface states that are highly consistent with our theoretical predictions.

In summary, we study the magnonic band structure and corresponding topological properties in antiparallelly aligned magnetic multilayers. We demonstrate that the long-range, chiral interlayer dipolar interaction generates bulk bands with nonzero Chern integers and ultralocalized surface states carrying chiral spin currents. The topology of the magnonic band can be switched between nontrivial and trivial phases through an external field. We also reveal that the multilayer system represents a magnonic implementation of the coupled wire model. We believe our study provides an easy-to-implement system for realizing topologically protected magnonic surface states and low-dissipation spin transport in a tunable manner, which is expected to benefit various areas of modern spintronics, particularly serving as an ultimate solution for on-chip nonreciprocal microwave components in both classical and quantum domains.

This work is supported by AFOSR under Grant No. FA9550-19-1-0048, and National Science Foundation under Grant No. DMR-2104912.

*zhongqhu@mit.edu

[1] M. Z. Hasan and C. L. Kane, Colloquium: Topological insulators, Rev. Mod. Phys. **82**, 3045 (2010).
[2] X.-L. Qi and S.-C. Zhang, Topological insulators and superconductors, Rev. Mod. Phys. **83**, 1057 (2011).
[3] Y. Ando and L. Fu, Topological crystalline insulators and topological superconductors: From concepts to materials, Annu. Rev. Condens. Matter Phys. **6**, 361 (2015).
[4] M. Sato and Y. Ando, Topological superconductors: A review, Rep. Prog. Phys. **80**, 076501 (2017).
[5] N. P. Armitage, E. J. Mele, and A. Vishwanath, Weyl and dirac semimetals in three-dimensional solids, Rev. Mod. Phys. **90**, 015001 (2018).
[6] P. Wang, L. Lu, and K. Bertoldi, Topological Phononic Crystals with One-Way Elastic Edge Waves, Phys. Rev. Lett. **115**, 104302 (2015).
[7] H. He, C. Qiu, L. Ye, X. Cai, X. Fan, M. Ke, F. Zhang, and Z. Liu, Topological negative refraction of surface acoustic waves in a weyl phononic crystal, Nature (London) **560**, 61 (2018).
[8] L.-H. Wu and X. Hu, Scheme for Achieving a Topological Photonic Crystal by using Dielectric Material, Phys. Rev. Lett. **114**, 223901 (2015).
[9] L. Lu, C. Fang, L. Fu, S. G. Johnson, J. D. Joannopoulos, and M. Soljačić, Symmetry-protected topological photonic crystal in three dimensions, Nat. Phys. **12**, 337 (2016).
[10] Y. Kajiwara, K. Harii, S. Takahashi, J. Ohe, K. Uchida, M. Mizuguchi, H. Umezawa, H. Kawai, K. Ando, K. Takanashi, S. Maekawa, and E. Saitoh, Transmission of electrical signals by spin-wave interconversion in a magnetic insulator, Nature (London) **464**, 262 (2010).
[11] L. J. Cornelissen, J. Liu, R. A. Duine, J. B. Youssef, and B. J. van Wees, Long-distance transport of magnon spin information in a magnetic insulator at room temperature, Nat. Phys. **11**, 1022 (2015).
[12] J. Han, P. Zhang, J. T. Hou, S. A. Siddiqui, and L. Liu, Mutual control of coherent spin waves and magnetic domain walls in a magnonic device, Science **366**, 1121 (2019).
[13] E. H. Turner, Interaction of Phonons and Spin Waves in Yttrium Iron Garnet, Phys. Rev. Lett. **5**, 100 (1960).
[14] B. Raquet, M. Viret, E. Sondergard, O. Cespedes, and R. Mamy, Electron-magnon scattering and magnetic resistivity in 3*d* ferromagnets, Phys. Rev. B **66**, 024433 (2002).
[15] S. R. Boona and J. P. Heremans, Magnon thermal mean free path in yttrium iron garnet, Phys. Rev. B **90**, 064421 (2014).
[16] S. Streib, N. Vidal-Silva, K. Shen, and G. E. W. Bauer, Magnon-phonon interactions in magnetic insulators, Phys. Rev. B **99**, 184442 (2019).
[17] L. Zhang, J. Ren, J.-S. Wang, and B. Li, Topological magnon insulator in insulating ferromagnet, Phys. Rev. B **87**, 144101 (2013).
[18] A. Mook, J. Henk, and I. Mertig, Edge states in topological magnon insulators, Phys. Rev. B **90**, 024412 (2014).
[19] S. A. Owerre, A first theoretical realization of honeycomb topological magnon insulator, J. Phys. Condens. Matter **28**, 386001 (2016).
[20] S. K. Kim, H. Ochoa, R. Zarzuela, and Y. Tserkovnyak, Realization of the Haldane-Kane-Mele Model in a System of Localized Spins, Phys. Rev. Lett. **117**, 227201 (2016).
[21] T. Hirosawa, S. A. Díaz, J. Klinovaja, and D. Loss, Magnonic Quadrupole Topological Insulator in Antiskyrmion Crystals, Phys. Rev. Lett. **125**, 207204 (2020).
[22] H. Kondo and Y. Akagi, Dirac Surface States in Magnonic Analogs of Topological Crystalline Insulators, Phys. Rev. Lett. **127**, 177201 (2021).
[23] R. Shindou, R. Matsumoto, S. Murakami, and J.-i. Ohe, Topological chiral magnonic edge mode in a magnonic crystal, Phys. Rev. B **87**, 174427 (2013).
[24] Y.-M. Li, J. Xiao, and K. Chang, Topological magnon modes in patterned ferrimagnetic insulator thin films, Nano Lett. **18**, 3032 (2018).
[25] X.-G. Wang, Y.-Z. Nie, Q.-L. Xia, and G.-H. Guo, Dynamically reconfigurable magnonic crystal composed of artificial magnetic skyrmion lattice, J. Appl. Phys. **128**, 063901 (2020).

[26] R. Matsumoto, R. Shindou, and S. Murakami, Thermal hall effect of magnons in magnets with dipolar interaction, Phys. Rev. B **89**, 054420 (2014).
[27] K. Shen, Magnon Spin Relaxation and Spin Hall Effect Due to the Dipolar Interaction in Antiferromagnetic Insulators, Phys. Rev. Lett. **124**, 077201 (2020).
[28] K. Yamamoto, G. C. Thiang, P. Pirro, K.-W. Kim, K. Everschor-Sitte, and E. Saitoh, Topological Characterization of Classical Waves: The Topological Origin of Magnetostatic Surface Spin Waves, Phys. Rev. Lett. **122**, 217201 (2019).
[29] J. Liu, L. Wang, and K. Shen, Dipolar spin waves in uniaxial easy-axis antiferromagnets: A natural topological nodal-line semimetal, Phys. Rev. Research **2**, 023282 (2020).
[30] S. Klingler, V. Amin, S. Geprägs, K. Ganzhorn, H. Maier-Flaig, M. Althammer, H. Huebl, R. Gross, R. D. McMichael, M. D. Stiles, S. T. B. Goennenwein, and M. Weiler, Spin-Torque Excitation of Perpendicular Standing Spin Waves in Coupled YIG/Co Heterostructures, Phys. Rev. Lett. **120**, 127201 (2018).
[31] J. Chen, C. Liu, T. Liu, Y. Xiao, K. Xia, G. E. W. Bauer, M. Wu, and H. Yu, Strong Interlayer Magnon-Magnon Coupling in Magnetic Metal-Insulator Hybrid Nanostructures, Phys. Rev. Lett. **120**, 217202 (2018).
[32] Y. Fan, P. Quarterman, J. Finley, J. Han, P. Zhang, J. T. Hou, M. D. Stiles, A. J. Grutter, and L. Liu, Manipulation of Coupling and Magnon Transport in Magnetic Metal-Insulator Hybrid Structures, Phys. Rev. Applied **13**, 061002(R) (2020).
[33] See Supplemental Material at http://link.aps.org/supplemental/10.1103/PhysRevLett.128.217201, which includes Refs. [34–36], for detailed derivations of the 2D and 3D magnonic Hamiltonian, as well as the independent micromagnetic simulation results.
[34] A. Berkowitz and K. Takano, Exchange anisotropy—a review, J. Magn. Magn. Mater. **200**, 552 (1999).
[35] M. H. Cohen and F. Keffer, Dipolar sums in the primitive cubic lattices, Phys. Rev. **99**, 1128 (1955).
[36] T. Holstein and H. Primakoff, Field dependence of the intrinsic domain magnetization of a ferromagnet, Phys. Rev. **58**, 1098 (1940).
[37] T. Yu, C. Liu, H. Yu, Y. M. Blanter, and G. E. W. Bauer, Chiral excitation of spin waves in ferromagnetic films by magnetic nanowire gratings, Phys. Rev. B **99**, 134424 (2019).
[38] J. Chen, T. Yu, C. Liu, T. Liu, M. Madami, K. Shen, J. Zhang, S. Tu, M. S. Alam, K. Xia, M. Wu, G. Gubbiotti, Y. M. Blanter, G. E. W. Bauer, and H. Yu, Excitation of unidirectional exchange spin waves by a nanoscale magnetic grating, Phys. Rev. B **100**, 104427 (2019).
[39] M. Ishibashi, Y. Shiota, T. Li, S. Funada, T. Moriyama, and T. Ono, Switchable giant nonreciprocal frequency shift of propagating spin waves in synthetic antiferromagnets, Sci. Adv. **6**, 6931 (2020).
[40] J. Han, Y. Fan, B. C. McGoldrick, J. Finley, J. T. Hou, P. Zhang, and L. Liu, Nonreciprocal transmission of incoherent magnons with asymmetric diffusion length, Nano Lett. **21**, 7037 (2021).
[41] W. P. Su, J. R. Schrieffer, and A. J. Heeger, Solitons in Polyacetylene, Phys. Rev. Lett. **42**, 1698 (1979).
[42] S. Klingler, A. Chumak, T. Mewes, B. Khodadadi, C. Mewes, C. Dubs, O. Surzhenko, B. Hillebrands, and A. Conca, Measurements of the exchange stiffness of YIG films using broadband ferromagnetic resonance techniques, J. Phys. D **48**, 015001 (2015).
[43] M. Langer, K. Wagner, T. Sebastian, R. Hübner, J. Grenzer, Y. Wang, T. Kubota, T. Schneider, S. Stienen, K. Lenz, H. Schultheiß, J. Lindner, K. Takanashi, R. E. Arias, and J. Fassbender, Parameter-free determination of the exchange constant in thin films using magnonic patterning, Appl. Phys. Lett. **108**, 102402 (2016).
[44] C. L. Kane, R. Mukhopadhyay, and T. C. Lubensky, Fractional Quantum Hall Effect in an Array of Quantum Wires, Phys. Rev. Lett. **88**, 036401 (2002).
[45] T. Meng, T. Neupert, M. Greiter, and R. Thomale, Coupled-wire construction of chiral spin liquids, Phys. Rev. B **91**, 241106(R) (2015).
[46] C. L. Kane and A. Stern, Coupled wire model of Z_4 orbifold quantum Hall states, Phys. Rev. B **98**, 085302 (2018).
[47] X.-C. Wu, C.-M. Jian, and C. Xu, Coupled-wire description of the correlated physics in twisted bilayer graphene, Phys. Rev. B **99**, 161405(R) (2019).
[48] J. H. P. Colpa, Diagonalization of the quadratic boson Hamiltonian, Physica (Amsterdam) **93A**, 327 (1978).
[49] L. Fu, C. L. Kane, and E. J. Mele, Topological Insulators in Three Dimensions, Phys. Rev. Lett. **98**, 106803 (2007).
[50] G. Gubbiotti, L. L. Xiong, F. Montoncello, L. Giovannini, and A. O. Adeyeye, Spin wave dispersion and intensity correlation in width-modulated nanowire arrays: A Brillouin light scattering study, J. Appl. Phys. **124**, 083903 (2018).
[51] V. Vlaminck and M. Bailleul, Current-induced spin-wave doppler shift, Science **322**, 410 (2008).
[52] A. Vansteenkiste, J. Leliaert, M. Dvornik, M. Helsen, F. Garcia-Sanchez, and B. Van Waeyenberge, The design and verification of mumax3, AIP Adv. **4**, 107133 (2014).